JOURNAL OF GEOPHYSICAL RESEARCH, VOL. 99, NO. B4, PAGES 6899–6912, APRIL 10, 1994

# Structure and tectonics in the region of flat subduction beneath central Peru: Crust and uppermost mantle

David E. James

Department of Terrestrial Magnetism, Carnegie Institution of Washington, D.C.

J. Arthur Snoke

Department of Geological Sciences, Virginia Polytechnic Institute and State University, Blacksburg

**Abstract.** Seismic waveform modeling of boundary interaction phases is used to determine the discontinuity structure of the crust in the Subandean and foreland-basin regions overlying the zone of flat subduction beneath east-central Peru. The data analyzed are from intermediate-depth earthquakes (110 to 155 km) recorded on an array of three-component short-period (1 Hz) digital seismographs deployed in the epicentral region. Full use is made of both P-to-S and S-to-P converted phases in the modeling. Results from the determination of crustal structure in the Subandean and foreland basin region of east-central Peru confirm the presence of vast depositional basins comprised of low velocity sediments up to at least 8 km thick which flank the Andean orogen to the east and correlate with a substantially thickened crust atop the Brazilian shield. Crustal thickness in the foreland basin varies from about 35 km or less where sedimentary cover is minimal to 44 km in regions of maximum sedimentary deposition. There is some evidence that the crust thins slightly on the western side of the foreland basin (in the gap between basin and Subandean fold and thrust belt), but it rapidly thickens to 45–50 km beneath the Subandes proper, and to more than 50 km in the southern part of the Subandean belt. The results are consistent with, but do not require, a thick-skinned model of foreland crustal deformation similar to that found for the block faulted terrane in Argentina above the zone of flat subduction there. At least some basin formation appears to be due to block faulting, where faults may penetrate into the mantle.

## Introduction

Lithospheric structure and tectonic evolution at the interface between the eastward migrating Andean orogen and the foreland basins situated atop the Brazilian shield have been the focus of several studies over the past decade [e.g., *Jordan et al.*, 1983; *Suárez et al.*, 1983; *Lyon-Caen et al.*, 1985; *Smalley et al.*, 1993]. Most of the recent studies have dealt with apparent thin-skinned crustal foreshortening in the Andean "hinterlands" of Chile and Argentina and the role of flexure and underthrusting of the Brazilian shield in those areas (see *Smalley et al.*, [1993] for a summary and references to earlier work). Research has involved chiefly the region of flat subduction in central Chile and Argentina, where the style of foreland deformation (thick-skinned block-faulted terrane of the Sierras Pampeanas of Argentine cratonward of the thin-skinned Precordillera (Subandean) thrust belt) has been cited as a tectonic characteristic in regions of flat subduction [e.g., *Smalley et al.*, 1993; *Fielding and Jordan*, 1988]. For the region of flat subduction in central Peru, the only direct evidence that bears on the style of fault tectonics in the foreland region east of the Subandean province comes from work by *Assumpção* [1992] who has shown using analysis of teleseismic waveforms of four events in the Serro do Divisor that fracture occurs along reverse faults at depths ranging from 26 to 42 km, indicatative of mantle-cored block faulting.

In this paper we present seismic results on crustal structure beneath the Subandean province of central Peru and the Ucayali basin which is situated to the east atop the Brazilian shield. The seismic analysis used to obtain crustal structure is based on waveform modeling of boundary interaction phases (mostly conversions) for nearby intermediate-depth events (110 to 155 km) recorded at eight three-component portable stations in central eastern Peru.

The general geologic and tectonic setting of the region of study within the central Andes is shown in Figure 1, and the relationship of the central Peru seismic



Paper number 93JB03112.
0148-0227/94/93JB-03112$05.00

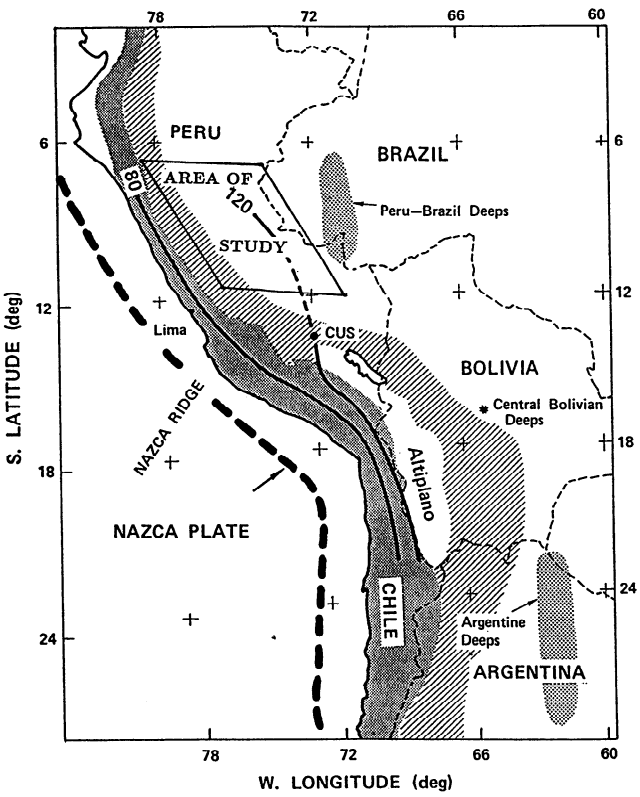


**Figure 1.** Generalized map of the central Andes showing area of study in relationship to subduction zone depths (heavy lines) and regions of deep focus earthquakes (stippled area). Approximate location of western (magmatic) cordillera is shown by stippled pattern, and location of eastern cordillera is shown by diagonal hatching.

array to the zone of flat subduction is shown in Figure 2. The area of study is situated above the easternmost extent of the area of flat subduction beneath Peru. A schematic cross section along line A-A′, from the trench to the Brazilian shield, is shown in Figure 3. The subducting Nazca plate beneath central Peru exhibits "normal" dip (≈ 30°) to about 100 km depth, where the slab proceeds subhorizontally for some 300 km before angling steeply downward ("resubducting") beneath the Subandean and Amazonian basin region of eastern Peru.

Figure 4 shows a schematic map of the principal geologic provinces, along with locations of seismic stations and earthquakes used in this study. The Ucayali basin and probably the Subandean belt overlie cratonic lithosphere of the Brazilian shield, with the Subandean province marking the farthest cratonward extension of the Andean orogen. By analogy with other regions, the sedimentary wedge of the Subandean zone is widely presumed to be overriding the foreland basement of the craton along thin-skinned décollement thrusts [e.g., *Jordan et al.*, 1983; *Beaumont*, 1981]. The Ucayali basin is one of the deep depositional foreland basins thought by some to have formed as a result of flexural downwarping of the Brazilian shield under the advancing Andean load [e.g., *Lyon-Caen et al.*, 1985; *Suárez et al.*, 1983]. The flexure model predicts that the bending of the overridden plate under the Andes will result in a gradually thickening sedimentary wedge from the edge of the exposed craton to the heel of the eastward migrating thrust belt of the Subandean province and in a progressively deepening Moho toward the orogen. As

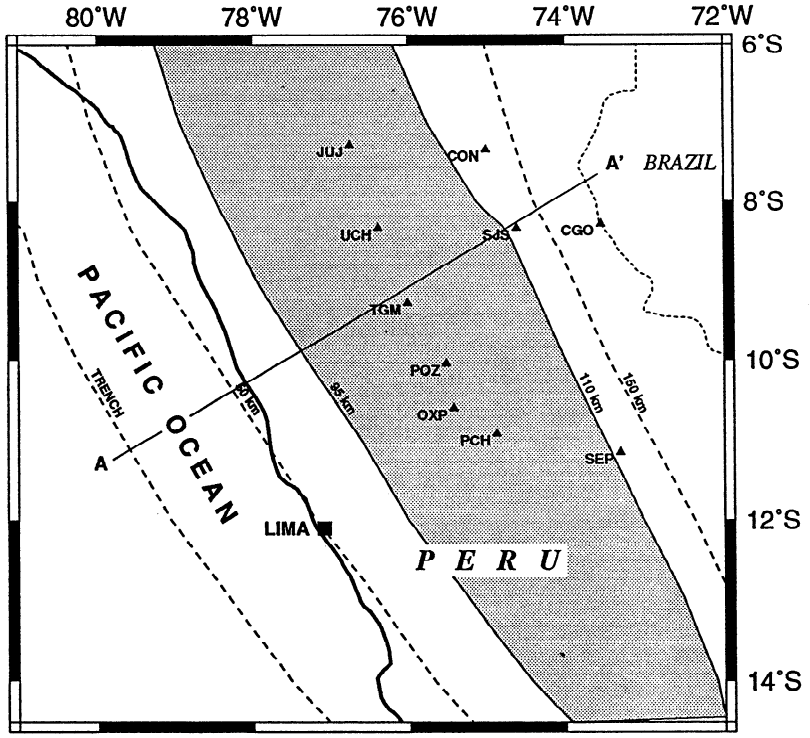


**Figure 2.** Map of area of study showing region of flat subduction (stippled pattern) in relation to station network. Position of trench and other Benioff zone contours are shown for reference. Stations are indicated by triangles. Line A-A′ marks line of cross section shown in Figure 3.

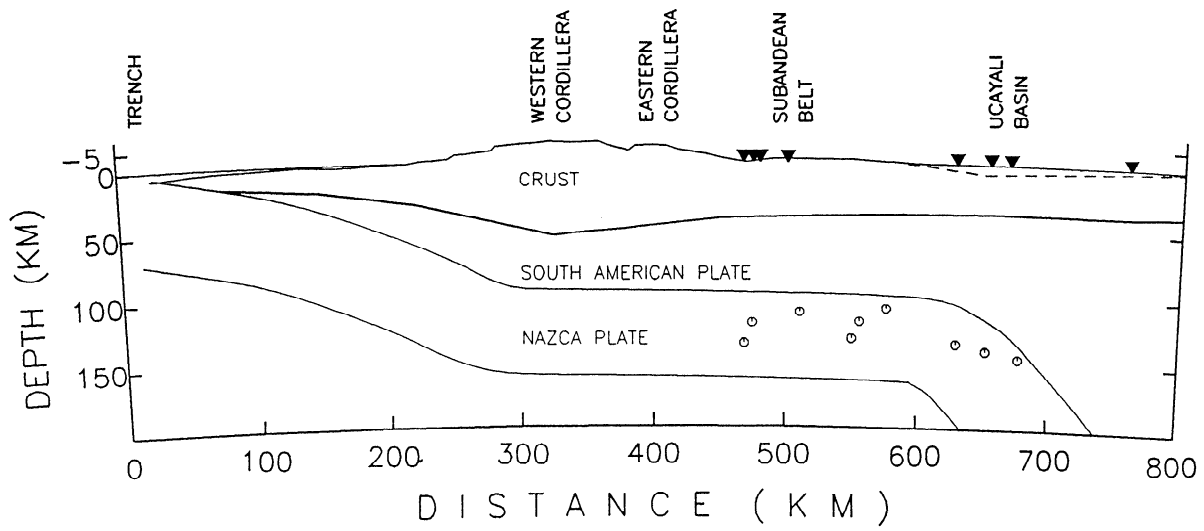


**Figure 3.** Schematic cross section along line A-A′ of Figure 2 showing the structure of the subduction zone and overlying continental lithosphere beneath central Peru (after E. O. Norabuena et al., accepted for publication, JGR, 1994). Projected station locations are shown as solid inverted triangles, and hypocenters are shown as open circles. Vertical scales above and below sea level are not the same.

we shall discuss below, neither our results on sedimentary layer thicknesses nor on Moho depths appear to be wholly consistent with predicted crustal characteristics of models based solely on simple lithospheric bending. In the remainder of this paper we will show how crustal structure is obtained from analysis of converted phases and the constraints imposed by that structure on possible tectonic models for the region.

## Data

The Department of Terrestrial Magnetism and the Instituto Geofísco del Perú in 1985 installed and op-

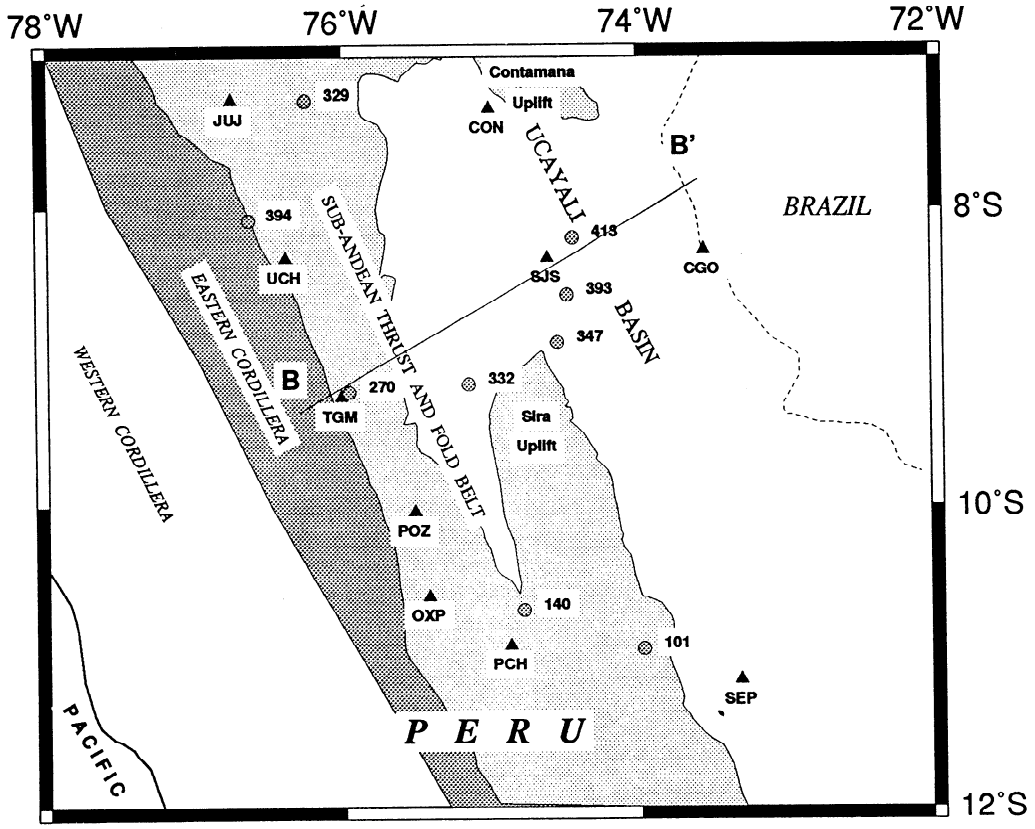


**Figure 4.** Location map for stations and epicenters of events used in this study. Principal geologic provinces are shown for reference. Line B–B′ gives trace of cross section shown in Figure 13.

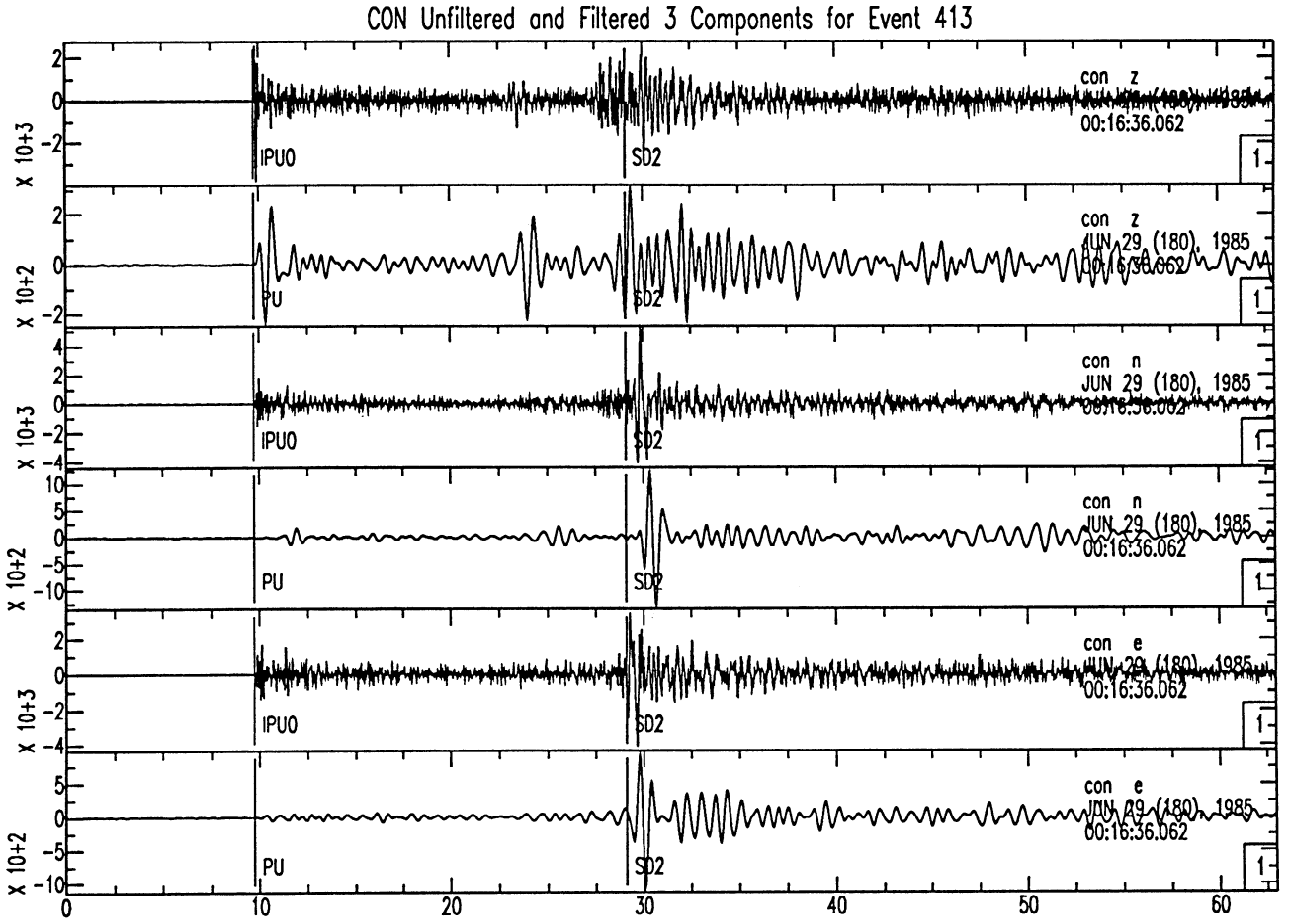


**Figure 5.** Example of vertical, radial and transverse unfiltered and filtered traces for station CON, event 413. Low pass filter is a six-pole Butterworth with corner at 2.0 Hz.

erated an array of portable digital seismic stations in the Subandean and Amazonian regions of east-central Peru. The array was operated for a period of 3 months (May 10 to August 4) during 1985, although the full array was in operation for only about 6 weeks. At maximum deployment, the network consisted of 15 three-component digital stations (see Figure 4). Instruments included eight University of Wisconsin portables with HS-10 1-Hz geophones, five Sprengnether DR-100s with L4-C 1-Hz geophones, and four Kinemetrics PDR-1s with SS-1 1-Hz geophones. The seismographs were all triggered instruments with sampling rates of 50 or 100 samples/s. Records include 4-10 s before trigger and 60-120 s of data after trigger, which is sufficient to include P and S wave direct arrivals as well as most of the more important boundary interaction phases following direct S. This study of boundary interaction phases utilizes only the University of Wisconsin instruments, which provided the most complete and reliable record set.

Analysis is based chiefly on observations of nine clearly recorded events (out of a catalog of over 70 well-observed

**Table 1.** Earthquake Locations and Origin Times

| Event | Year | Day | Origin Time, UT | Latitude, deg | Longitude, deg | Depth, km | RMS Residual |
|---|---|---|---|---|---|---|---|
| 101 | 1985 | 152 | 0435:55.1 | -10.96 | -73.98 | 110 | 0.30 |
| 140 | 1985 | 155 | 0821:39.2 | -10.70 | -74.79 | 113 | 0.31 |
| 270 | 1985 | 165 | 0621:42.6 | -9.23 | -75.96 | 121 | 0.38 |
| 329 | 1985 | 170 | 0248:53.7 | -7.28 | -76.25 | 133 | 0.34 |
| 332 | 1985 | 170 | 0624:22.8 | -9.18 | -75.16 | 120 | 0.36 |
| 347 | 1985 | 172 | 0109:14.1 | -8.90 | -74.55 | 136 | 0.23 |
| 393 | 1985 | 176 | 0747:32.1 | -8.58 | -74.49 | 141 | 0.28 |
| 394 | 1985 | 176 | 1018:16.3 | -8.08 | -76.65 | 137 | 0.29 |
| 413 | 1985 | 180 | 0016:20.5 | -8.20 | -74.44 | 146 | 0.23 |

Times are in seconds.

intermediate-depth earthquakes) which are located in the region of flat subduction and resubduction and whose epicenters lie within the boundaries of the network. The earthquakes have been located using HYPOELLIPSE [*Lahr*, 1992] as modified by J. A. Snoke and J. C. Lahr. Modified HYPOELLIPSE uses travel-time tables for spherical-Earth models in which Poisson's ratio can vary with depth and velocity gradients are allowed within layers. An optimal velocity-depth model was obtained by trial and error, and station residuals were introduced to accommodate lateral variations in crustal and sedimentary thickness at each station. Results are shown in Table 1. Formal ($1\sigma$) location errors are typically less than 3 km (mostly in depth), origin time errors less than 0.3 s, and RMS residuals about 0.3 s. Details on the method and results of hypocenter locations are discussed in more detail in *Norabuena et al.*, [1994].

The source mechanisms for the intermediate-depth events used in this study appear to be remarkably clean and impulsive for both P and S waves. In addition, the absence of a low-Q region above the slab results in only minimal attenuation for S waves. Nonetheless, the short-period nature of the recording system includes considerable unwanted high-frequency energy. The seismograms are therefore low-pass-filtered (six-pole Butterworth) with a corner at 2 Hz, a process which substantially enhances the signal-to-noise ratio of the converted and reflected boundary interaction phases as shown in Figure 5.

## Methodology

We use a modified version of the deterministic analytical technique complete ordered ray expansion (CORE) which was developed by T. J. Clarke and is described by *Clarke and Silver*, [1991]. As in CORE, we begin with an assumed laterally homogeneous spherical-Earth velocity structure, a previously determined hypocenter and focal mechanism, and a pulse shape based on the first few cycles of the vertical component direct P arrival. From this information, synthetics are generated using the geometrical ray theory approximation [e.g., *Chapman*, 1976]. A focal mechanism is chosen that matches the polarities and relative amplitudes from among P, SV, and SH. For these events the dominant contribution is from a single-sided pulse with a duraton of less than 0.2 s. Unlike CORE, we do not generate a catalog of all possible boundary interaction phases but, for efficiency, generate only those conversions and reflections likely to be observable. (Test runs were done first with CORE to determine which phases to include.) A single source-time function is used to generate all arrivals, with the only difference in pulse shape coming from differing attenuation. Q for both P and S is specified for each layer, and a causal Q filter is used.

As with CORE, the first stage of analysis requires obtaining a smooth velocity model that predicts correctly the travel times of the main (direct) phases for each station-event pair. In the present study, most of the mismatch between predicted and observed S-P differential travel times appears to be the result of errors in hypocenter location rather than velocity variation. We therefore constrain the main phases on the synthetics to match those on the observed seismograms by introducing small perturbations in focal depth or epicentral distance. These perturbations have a negligible effect on differential travel times between boundary interaction phases and the main phases from which they are produced and thus have no effect on the modelling.

The second step in the analysis involves waveform fitting of the secondary (boundary interaction) phases to obtain estimates of differential travel times between arrivals. The data set contains no well-constrained reflected boundary interaction phases, so that estimates are only for S-P differential travel times within each layer. To first order, direct S minus an S-to-P conversion gives provides the same information as P-to-S minus direct P. Hence for each layer we have a differential travel time constraint that applies to three variables: layer thickness, $V_p$, and Poisson's ratio. The $V_p$ model is assumed, so either layer thicknesses or Poisson's ratios can be estimated. Our concern here is primarily with layer thickness, and our work confirms the finding of *Clarke and Silver* [1993] that layer thicknesses are better constrained than Poisson's ratios.

Because of the impulsive character of the seismic signals, we use simple visual correlation for phase matching between data and synthetics. We estimate that phase correlations are accurate to better than a tenth of a second, which, for fixed $V_p$ and velocity ratio, implies an uncertainty in layer thickness of about 0.4 km.

Stacking of events is precluded by a combination of factors, notably that station/event geometry is significantly different for almost every seismogram of the Peru data set and that layer thicknesses can vary substantially in a relatively small area. Because stacking is not possible with our data and because the observed boundary interaction phases are so well defined, we have opted not to use formal inversion but rather to perturb interface depths by trial and error to optimize the fit between data and synthetics.

In the notation used here, lowercase indicates upward traveling wave, except for direct arrivals which are always capital. Internal boundaries within the crust are designated by number with the shallowest being boundary "1", and the Moho is specified by the letter "*m*". Examples: *pms* signifies a phase that starts out as an upward traveling P wave which is converted to an upward traveling S wave at the Moho, and *smp1s* is an S-to-P conversion at the Moho followed by a P-to-S conversion at the base of the uppermost crustal layer (henceforth termed layer1).

## Analysis of Data

Boundary interaction phases have been analyzed for arrivals at four stations in the East Peru Basin (CON, CGO, SJS, and SEP) and for four stations in the Suban-

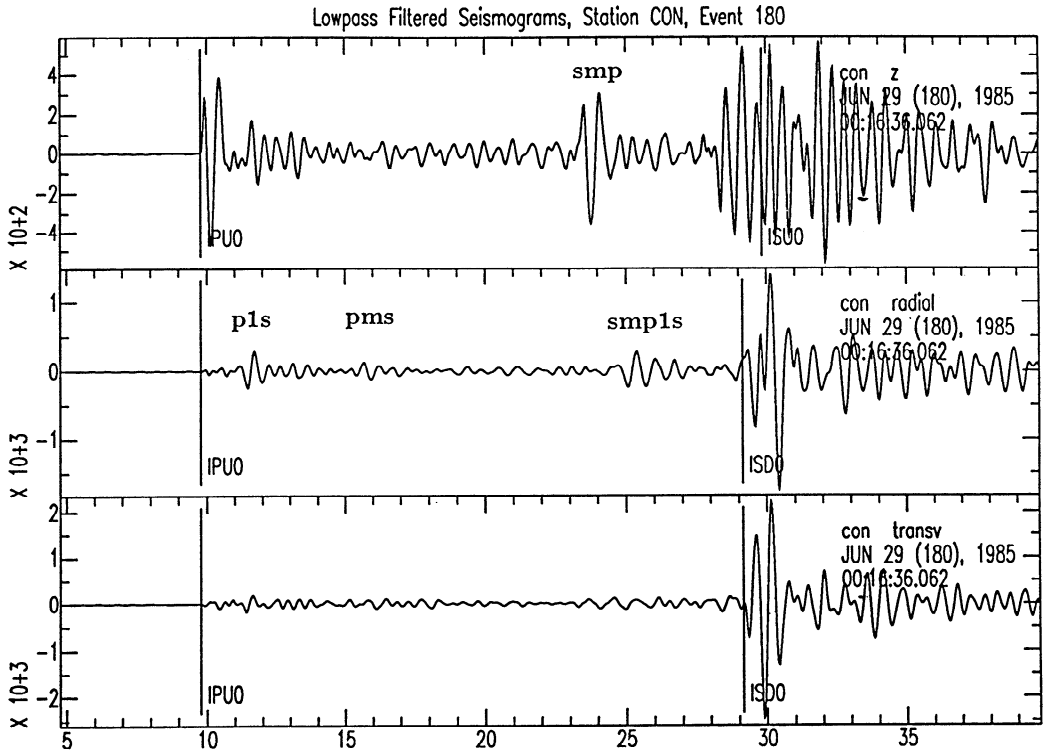


**Figure 6.** Filtered traces as in Figure 5, truncated just before direct S, with direct P and the prominent boundary interaction phases marked for reference. S-to-P conversions appear on the vertical component, whereas P-to-S conversions are largest on the radial component. Note the double conversion, *smp1s* (S-to-P at Moho, P-to-S at base of sedimentary layer), present at about 15 s on the radial component.

dean belt (JUJ, UCH, TGM, and POZ) (see Figure 4). Major boundary interaction phases at each station were identified by comparing a number of seismograms for different events observed at the station with synthetic seismograms for appropriate layered-Earth models. Once the major features of the seismograms were identified, the discontinuity structure was refined, and matching synthetics were obtained for each station/event pair. Although several boundary interaction phases that occur in the time interval immediately following the direct S wave arrival have large predicted amplitudes, the arrivals are both too numerous and too poorly separated in time to warrant their inclusion in the modeling. The analysis here is therefore confined to phases that arrive between direct P and direct S.

Low-pass-filtered seismograms for an event/station pair in the Ucayali basin and an event/station pair in the Subandean zone are shown in Figures 6 and 7, respectively. The traces are truncated just prior to the arrival of direct S to enhance the visibility of pre-S arrivals on the radial component. Identified boundary interaction phases have been labeled. An important feature of Figure 6 (Ucayali basin) is the virtual absence of P wave arrivals (including direct P) on the radial component and the absence of pre-S shear wave arrivals on the vertical component. These observations are consistent with extremely low near-surface velocities as discussed below. Strong P-to-S and S-to-P conversions are observed on the radial and vertical components, respectively. In Figure 7 (Subandean region) the vertical component seismogram displays similar S-to-P conversions to those seen in Figure 6, although for the example shown in Figure 7, *smp* is notably smaller relative to *s1p*. On the other hand, the radial component seismogram in Figure 7, which is characteristic of many recorded at Subandean stations, contrasts significantly with that shown in Figure 6. The differences include the clear presence of P and *s1p* on the radial component (suggesting much higher near-surface velocities in the Subandean region) and the virtual absence of P-to-S conversions from either the Moho or the upper crust.

Two major discontinuities characterize the continental crust beneath eastern Peru: (1) the base of a low-velocity surface sedimentary layer (layer1) and (2) the Moho. The crystalline middle and lower crust appears to be essentially transparent, with no major discontinuities. Differential travel times between converted phases and direct phases are used in conjunction with assumed layer velocities to estimate the approximate thickness of the upper sedimentary layer (layer1) and of the crust for each event/station pair.

Crustal velocities are chosen to be typical for the rock types involved but are otherwise poorly constrained by our data. (Thus velocity-depth models should be viewed primarily as time-equivalent depth sections.) Layer velocities are assumed to be laterally homoge-

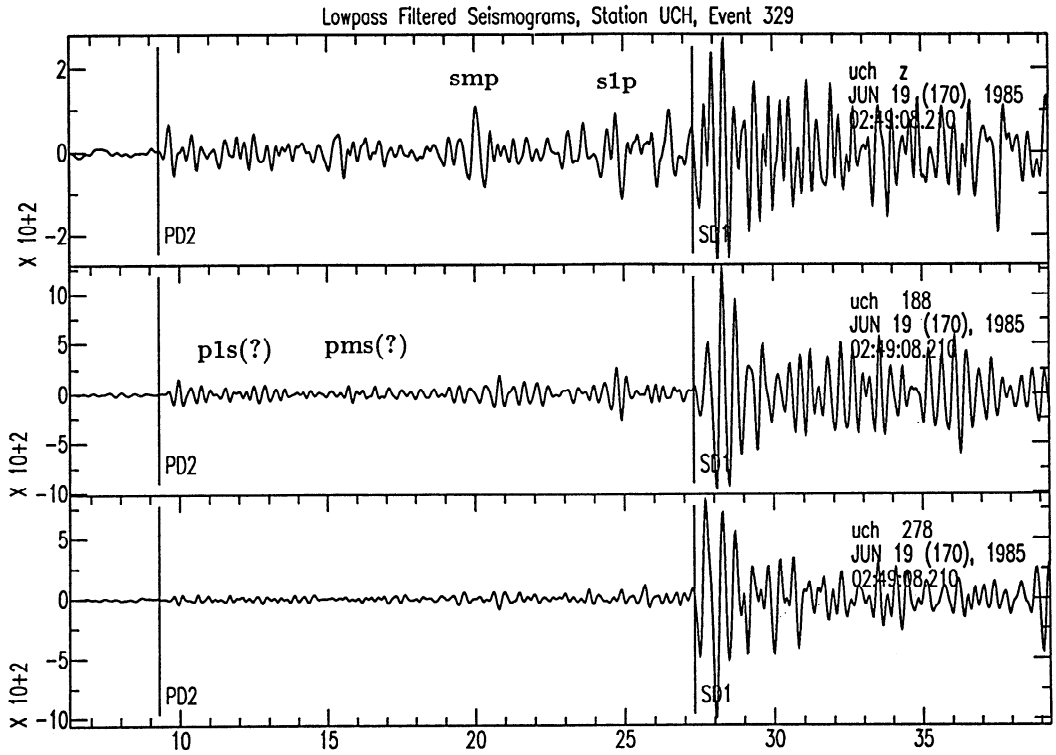


**Figure 7.** Filtered traces of seismograms from Subandean station POZ for event 332. While S-to-P conversions are relatively large amplitude on the vertical component, the corresponding P-to-S conversions on the radial component are small or absent. In general, seismograms of Subandean stations are considerably more complex than those of the Ucayali basin stations.

neous within the given geologic province, either the foreland basin or the Subandes. In the East Peru basin, layer1 corresponds to the base of the thick clastic sedimentary section which is the result of infilling of sediments shed from the Andean orogen. On the basis of velocity measurements of similar sedimentary rock types [e.g., *Waters*, 1987; *Christensen*, 1982], we assume a P wave velocity 2.2 km/s at the top of the sedimentary layer and that velocity increases linearly to 4.0 km/s at the contact with crystalline basement. We have assumed a Poisson's ratio of 0.30, a value typical of continental sediments of the type present in eastern Peru. We assume a P wave velocity of the crystalline basement of 6.4 km/s at 20 km depth, increasingly linearly to 6.6 km/s at the base of the crust. Velocities above 20 km are constrained by assuming a linear gradient of 0.04 km/s/km from the top of the layer down to 20 km depth. We take Poisson's ratio for the crystalline crust of the underlying Brazilian shield to be 0.27, a typical value for crust in shield areas [e.g., *Mooney and Braile*, 1989].

Synthetics based on the above model cannot explain the total absence of direct P on radial component records for stations in the Ucayali basin (e.g., Figures 5 and 6). The assumed P-wave velocity of 2.2 km/s at the surface is low even for sedimentary rocks, although unconsolidated sediments or weakened sedimentary rocks can have velocities as low as 1 km/s or less. While we lack detailed information about rock types beneath the stations, observations made at the time of station installation indicate that the first several meters are unconsidated sediments. We have accordingly included in our velocity model for the Ucayali basin a thin layer of unconsolidated sediments: $V_p$ is assumed to be 300 m/s at the surface increasing linearly to 2.2 km/s at 100 m depth. Tests using Haskell synthetics verify that no conversions or reverberations need be included if we do not try to model in detail the waveform on the radial preceding *pls*.

For the Subandean stations, layer1 conversions are more elusive. In some instances there may be more than one crustal discontinuity involved, although we have modeled only one here, taken to be the base of the thrust stack (decollement?). The sedimentary rocks above layer1 in the Subandean zone tend to be somewhat metamorphosed and are certainly higher velocity than the deposits found in the Ucayali basin. We assume a P wave velocity of 4.0 km/s at the surface in the Subandean zone, increasing linearly to 5.0 km/s at contact with basement. Velocities in the crystalline basement beneath the Subandes are assumed to be the same as for the Ucayali basin. Examples of typical velocity-depth models for each of the two regions are shown in Figure 8.

Results of waveform fitting are given for each station/event pair in Table 2. Except for stations SEP (malfunctioning E-W component) and JUJ (too distant from most events), at least two events were analyzed for each station. In many instances, either the P-to-S or the S-to-P conversion is superior in quality to

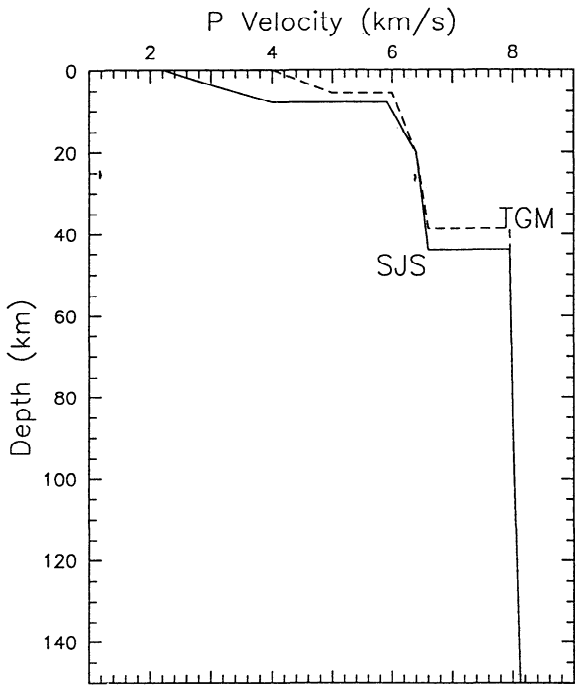


**Figure 8.** Examples of typical velocity-depth models for Ucayali basin station, SJS, and a Subandean station, TGM, showing particularly the much lower velocities of the upper crustal sedimentary layer in the Ucayali basin. Because of the depth scale used, the low velocities assumed for the first 100 m beneath the Ucayali basin cannot be resolved.

the other, in which case the clearest converted phase is used for determining layer thickness. In cases for which both phases are of good quality, both can be used in the modeling, but it must be taken into account that the conversion points for S-to-P and P-to-S differ geographically by a few kilometers for layer1 conversions and by tens of kilometers for Moho conversions. This necessitates creating separate synthetics for each case.

The observed vertical and radial component seismic records and corresponding synthetic waveforms for the Ucayali basin stations are shown in Figure 9, and those for the Subandean stations in Figure 10. In general, our waveform inversion is for S-to-P conversions which are typically more prominent than the corresponding P-to-S conversions. In fact, the *smp* Moho conversion for some events at CON and CGO are so large that a sizeable P-to-S secondary conversion is produced at the layer1 discontinuity. That phase, *smp1s* (see Figure 6), is clearly observed on the radial component for a number of records and was originally misidentified as a P-to-S converted phase from a mantle discontinuity. The secondary conversion does, however, prove beyond doubt that *smp* is correctly identified on the seismograms. Interestingly, station SJS, situated near the axis of the Ucayali basin, consistently exhibits very clear P-to-S conversions but only rarely S-to-P conversions of comparable quality. We have no ready explanation for this feature, although it could be due to a dip in the Moho near the station.

The quality of the boundary interaction phases for the Subandean stations is less consistently good, especially for layer1, than for the basin stations. In general, a single upper crustal discontinuity appears to fit most of the data reasonably well, although there is evidence of greater complexity in some records, e.g., UCH/332. The Moho conversions are quite clear on many of the records, indicating that the discontinuity is sharp beneath the Subandean zone as well.

Model depths to the base of the sedimentary layer beneath the Ucayali basin and model depths to the Moho beneath the entire region are shown as contoured quantities in Figures 11 and 12, respectively. The velocity models used for obtaining depths are as described

**Table 2.** Layer1 and Crustal Thicknesses by Station/Event Pair

| Station/Event | *s1p* | *p1s* | *smp* | *pms* |
|---|---|---|---|---|
| | | *Ucayali Basin* | | |
| CON/332 | 6.5 | 4.8 | | 38.5 |
| CON/393 | 5.0 | 5.0 | 37.0 | |
| CON/413 | 4.0 | 4.0 | 33.0 | 34.0 |
| CGO/393 | 3.4 | 3.4 | 42.0 | |
| CGO/413 | 2.6 | 2.6 | 41.0 | |
| SJS/270 | 6.9 | 8.1 | | 43.5 |
| SJS/332 | 7.3 | 7.7 | 44.0 | 44.0 |
| SJS/347 | 7.3 | 8.0 | | 44.0 |
| SEP/101 | 4.6 | | 34.5 | |
| | | *Subandean Zone* | | |
| UCH/332 | 13.8 | | 40.2 | |
| UCH/329 | 14.0 | | 48.0 | |
| UCH/394 | 16.7 | | 48.7 | |
| TGM/332 | 5.5 | | 38.5 | 38.5 |
| POZ/140 | 4.0 | | 54.8 | |
| POZ/332 | 7.2 | | 46.0 | |
| JUJ/394 | 15.5 | | 46.0 | |

Thicknesses are in kilometers and all times are in seconds.

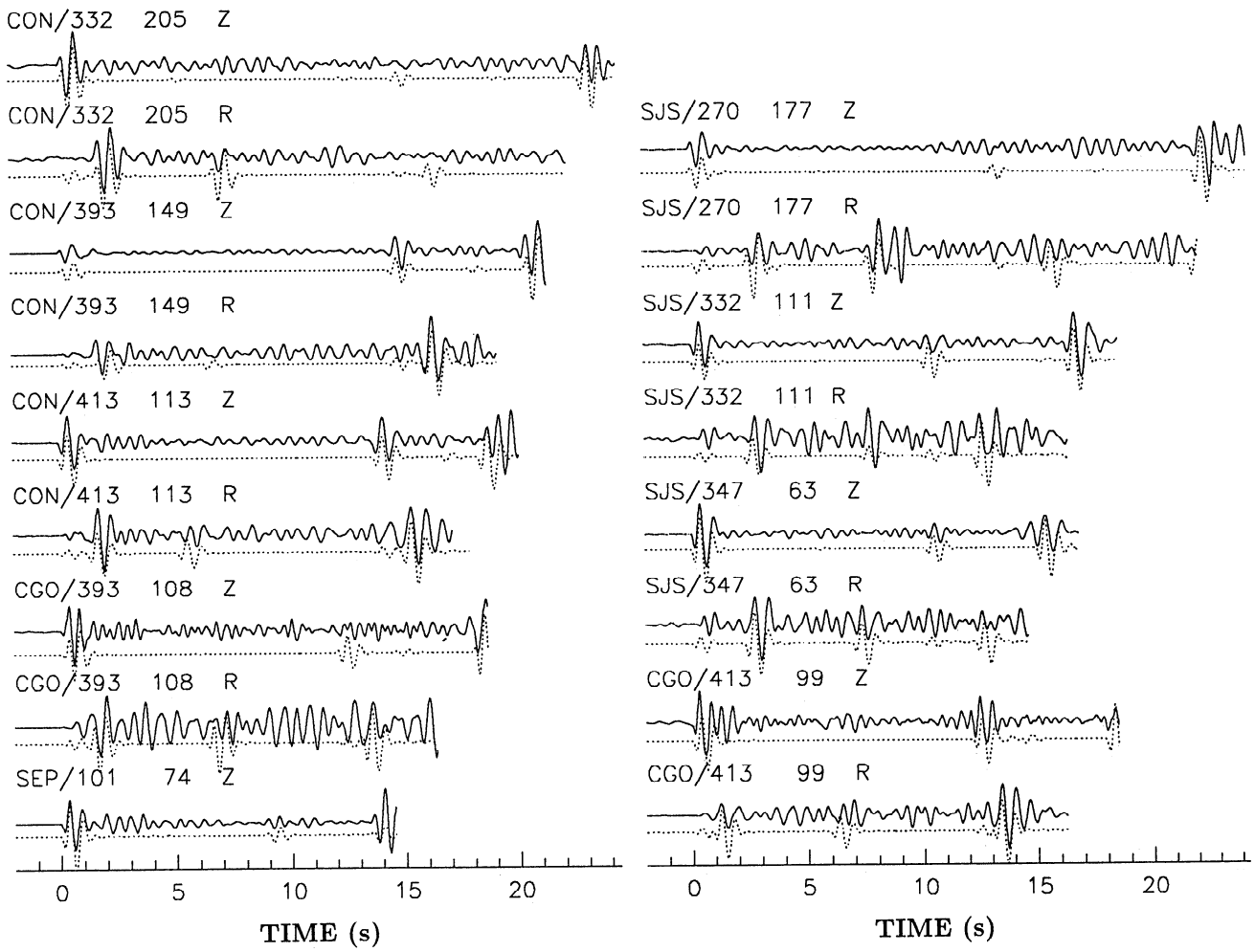


**Figure 9.** Observed and synthetic seismograms for the Ucayali basin for event/station pairs used in this study. The records are truncated just prior to onset of the S wave: the arrivals at the tail end of a number of records are *s1p* conversions. Notation above each trace gives the station/event pair, the epicentral distance of the event from the station in kilometers and the component (Z or R). All traces are low-pass-filtered as in Figures 6 and 7.

above. In general, we consider the velocities used for the upper crustal layer within the Ucayali basin to be toward the low end of plausible values [e.g., *Waters*, 1987; *Christensen*, 1982]; hence the calculated thicknesses of layer1 are likely to be lower bounds on actual thicknesses.

## Layer1

**Ucayali basin.** The Ucayali basin is an area of massive clastic deposition, an apparent consequence of continuing subsidence associated with miogeosynclinal sedimentation on the eastern flank of the Andes dating back perhaps to the Paleozoic [*Ham and Herrera*, 1963; *Räsänen et al.*, 1987]. The bulk of the sediments that make up the Ucayali basin and other Amazonian basins of the region are continental fluvial deposits deposited in the basin during the Tertiary Andean orogenies [*Räsänen et al.*, 1987]. Räsänen et al. suggest that there has been a total aggradation of 4 to 11 km of deposits in the subsiding basins flanking this region of the Andes.

The greatest thickness of the sedimentary section (layer1) in the Ucayali basin determined in this study, about 8 km, is in the vicinity of station SJS near the axis of the basin as shown on the isopach map in Figure 11. The calculated thickness of the sedimentary section is inferred from seismic travel times and the assumed seismic velocity structure for the sedimentary rocks as discussed near the end of the previous section. Any adjustment in the assumed velocities will of course produce a corresponding change in the calculated layer1 thicknesses.

Depth to the base of the sedimentary section decreases in all directions away from SJS. In the vicinity of station CON, on the SW flank of the Contamana Uplift, sedimentary rocks aggregrate about 4 to 5 km. Similarly, at station CGO on the western flank of the Serro do Divisor and almost due east of SJS, total thickness of the sedimentary column is only about 3 km. Station SEP, which is situated well to the south and on the axis of the Ucayali basin near its southern extent, is underlain by about 4.6 km of sedimentary rocks.

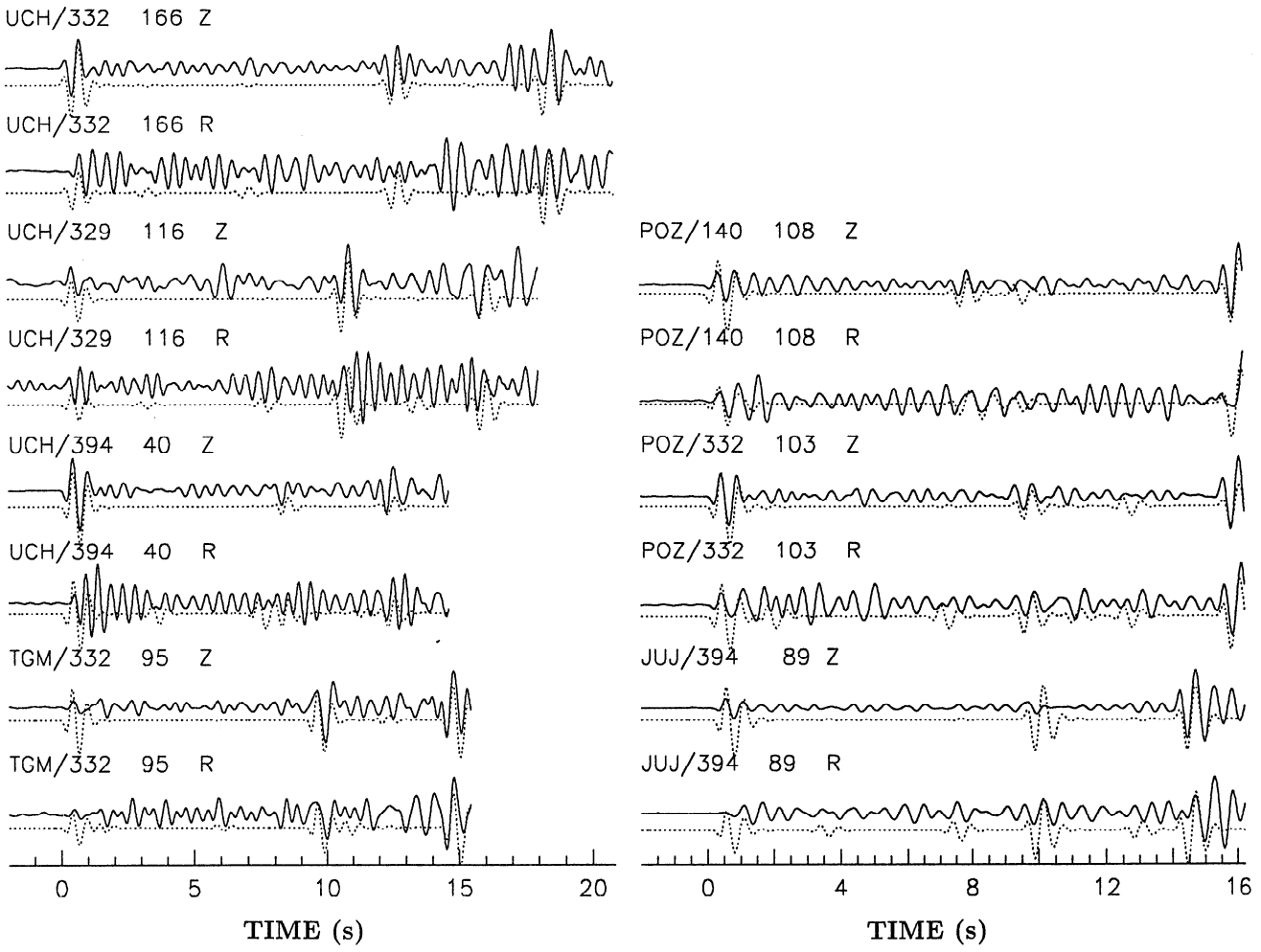


**Figure 10.** Observed and synthetic seismograms for the Subandean zone for event/station pairs used in this study. See Figure 9 caption for further explanation.

**Sub-Andean zone.** The seismic results for stations in the Subandean belt are predictably somewhat less clear-cut than they are for those of the Ucayali basin. The conversions are not as strong nor as consistent, and they tend to be evident mostly on the vertical component as arrivals resulting from S-to-P conversions. The sedimentary/crystalline boundary is hence not as well defined or as simple as in the Subandean region, although there is ample evidence that a regional discontinuity does exist there.

Given the sparseness of data and variability of thickness, we have made no attempt to contour layer1 beneath the Subandean belt. Depths to the base of layer1 are strongly bimodal as shown in Figure 11, with values around 15 km for the northerly two stations and about 5–6 km for the southerly two stations. If the layer1 discontinuity is associated with a décollement surface, substantial relief is implied for that thrust surface along the strike of the Andes. It may be relevant that the southern stations, TGM and POZ, are relatively close to the eastern edge of the thrust belt whereas the northerly stations, JUJ and UCH, are situated farther to the west.

## Crustal Thickness

Depths to Moho are contoured in Figure 12. The M-discontinuity is sharp and unambiguous throughout the region of study. While we have observed clear conversions for both *pms* or *smp* at all stations, the stations with the best observations, as for layer1, are again those in the Ucayali basin. Typically, the best observed phases are *smp*, with the notable exception of station SJS, where *smp* is relatively weak but *pms* is unusually prominent and consistently well observed for a large number of events (see SJS radial components in Figure 9).

If we assume that crustal thickness varies smoothly between points where Moho depth is well determined, then structure on the Moho beneath the Ucayali basin appears to vary in a systematic way. Station SJS which is close to the axis of the Ucayali basin is, as shown above, underlain by a substantially thicker sedimentary section than is found for any other station in the region. It is therefore not surprising that crustal thickness is correspondingly greater. The SJS events (all

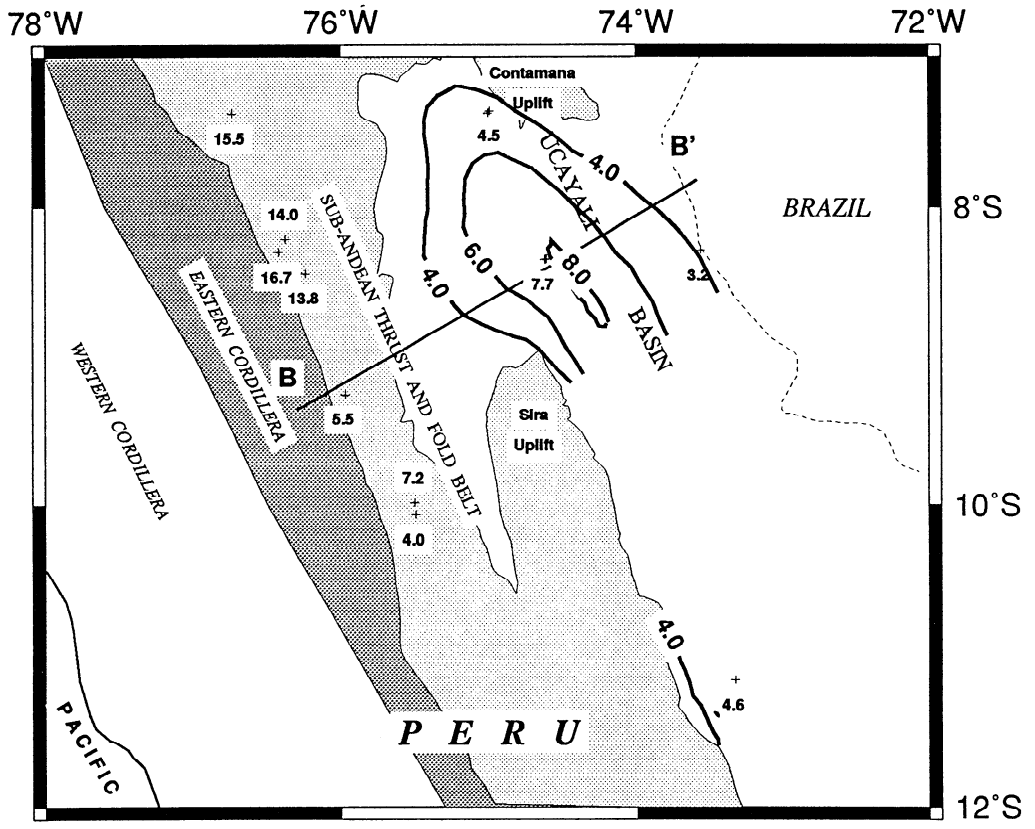


**Figure 11.** Contour map showing thickness of the sedimentary layer of the Ucayali basin based on S-to-P and P-to-S converted phases. Contours are shown as heavy solid lines and depths are given in kilometers for each contour. Conversion points are shown by crosses, and the corresponding depth is indicated for each point. To reduce clutter, not all conversion points given in Table 2 are included.

to the south or southwest) for which we have reliable Moho conversions yield comparable crustal thicknesses of about 44 km. The crust is thinner (about 35 km) at stations CON near the Contamana uplift, at station CGO (41 km) near the Serro do Divisor, and at station SEP (35 km) in the southernmost part of the Ucayali basin. The pattern of crustal thinning in all directions from SJS is consistent with depression of the Moho in response to the clastic load at the surface.

From the Ucayali basin westward (toward the orogen), the crust thins to less than 40 km near the boundary between the Subandean zone and the east Peru basin but then thickens rapidly beneath the Subandean zone and into the eastern cordillera. From the region of generally thinner crust around TGM, moreover, there is an increase in crustal thickness southward through POZ and toward the hinge area where the Andes begin to widen into what, at about 13.5°S latitude, is termed the Pisco deflection. The Andes achieve their maximum width and crustal thickness south of that deflection [*James*, 1971]. The deflection also marks the principal latitudinal segmentation boundary of the central Andes where the mean trend changes from about N35° W to N50° W [*Mégard*, 1987]. It would appear likely that crustal thickening near POZ and south signals a regional trend of increasing crustal thickness in the direction of the altiplano.

## Discussion and Conclusions

The seismic measurements of crustal structure presented in this paper confirm the presence of a vast sedimentary basin flanking the Subandean province to the east. The contact between the sedimentary section and the underlying crystalline basement of the Brazilian shield is a major seismic discontinuity. The Ucayali basin, the principal site of sedimentary deposition, is composed of up to 8 km or more of low-velocity sedimentary rocks. The area of maximum sedimentary thickness also corresponds to the region of maximum crustal thickness in the Ucayali basin, with crustal thickness decreasing in all directions from the axis of the sedimentary basin. Westward from the basin axis (toward the Andes) the crust thins slightly before thickening rapidly toward the eastern cordillera and especially toward the altiplano to the south.

The seismic results are remarkably consistent with the geologic synthesis of the region published nearly 30 years ago by *Ham and Herrera* [1963], as well as with recent summaries by *Räsänen et al.* [1987] and *Jordan*

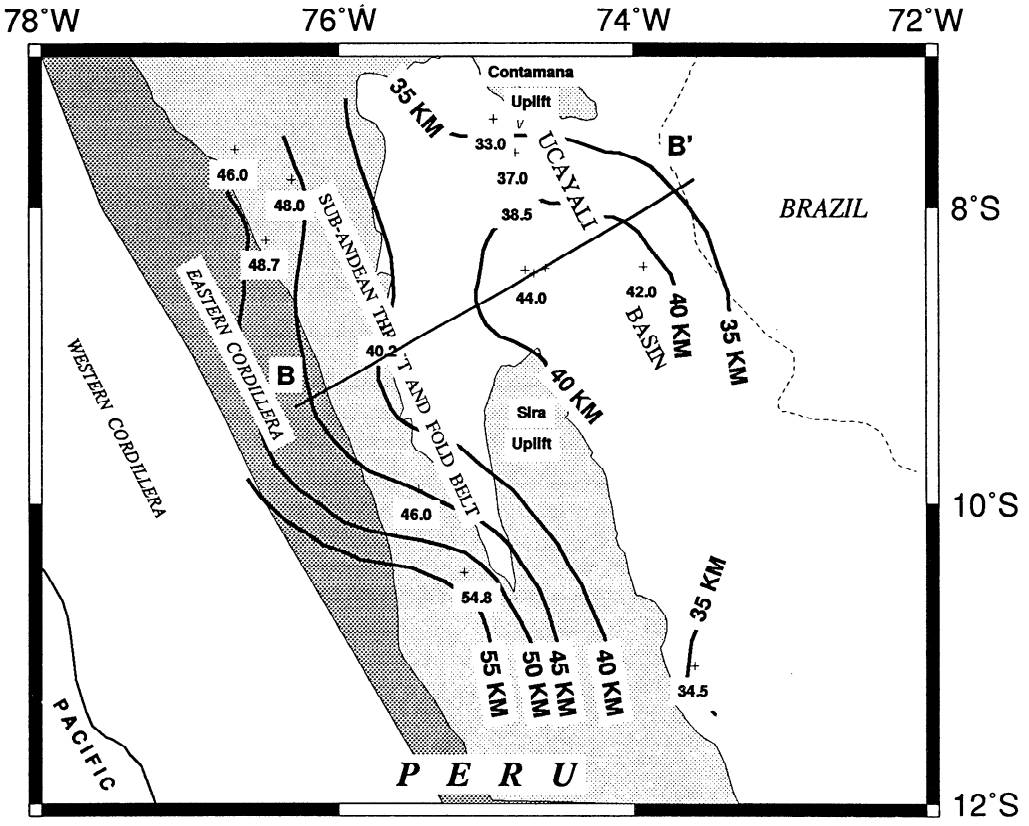


**Figure 12.** Contour map of crustal thickness beneath the region of study based on converted phases. Contours are shown as heavy solid lines and are based on an assumption of long-wavelength variation in crustal thickness between points where depth has been computed. Points of conversion at the Moho are shown by crosses, and the computed depth to Moho at each point is indicated. To reduce clutter, not all conversion depths given in Table 2 are shown.

*et al.* [1983]. All of the important uplifts, including the Serro do Divisor, and the Contamana and Sira uplifts which flank the Ucayali basin to the east, north, and southwest, respectively, are bordered by extensive fault systems, most of which were interpreted by Ham and Herrera to be basement-cored westward dipping reverse faults. There is direct evidence at least for the Serro do Divisor uplift that the faulting is of the thick-skinned variety, with reverse faults extending well into the mantle as shown by *Assumpção* [1992]. While the seismic data presented in this paper are too sparse to allow a definitive interpretation of the tectonic style of faulting, the three-dimensional pattern of crustal thickness and sedimentary thickness is consistent with thick-skinned tectonics.

The seismic results of upper crustal structure in the Subandean region are far less definitive than are those for the Ucayali basin. The large-scale faulting of the Subandean region produces vast structural complexity that is not readily amenable to seismic interpretation. It is therefore rather surprising that the data do exhibit clear evidence of a single (or in some cases, a double) upper crustal discontinuity. The depth of the discontinuity changes dramatically across the region, however, from rather shallow (4 to 7 km) in the southern Subandean region to 14 to 17 km in the northern part of the region. Station spacing is too sparse to determine if the change in depth is gradual or abrupt. By analogy with other Subandean regions in northwest Argentina and Chile where the seismotectonics is better known, we have interpreted the layer1 boundary in the Subandean region to be a basil décollement along which low-angle thrusts at the base of the sedimentary section have coalesced [e.g., *Mingramm et al.*, 1979; *Jordan et al.*, 1983; *Allmendinger et al.*, 1990].

An interpretive summary of our results is shown as a cross section in Figure 13. The section corresponds approximately to line B–B' shown in Figure 4. While the tectonic structures shown in the Figure 13 cross section are highly speculative, the model is consistent with the results we have obtained in this study. Principal conclusions from this study are as follows: (1) The Ucayali basin is a region of active subsidence, with sedimentary sections of at least 8 km and corresponding crustal thickness of about 44 km. The results are in good agreement with cross sections shown by Ham and Herrera, where the axis of the Ucayali basin contains up to 10 or 12 km of sedimentary rocks. (2) The sedimentary section beneath the Ucayali basin thins to the north and east, as does the crust as a whole. The thinning of both sediments and crust off the axis of the Ucayali basin could suggest either flexure associated with sub-

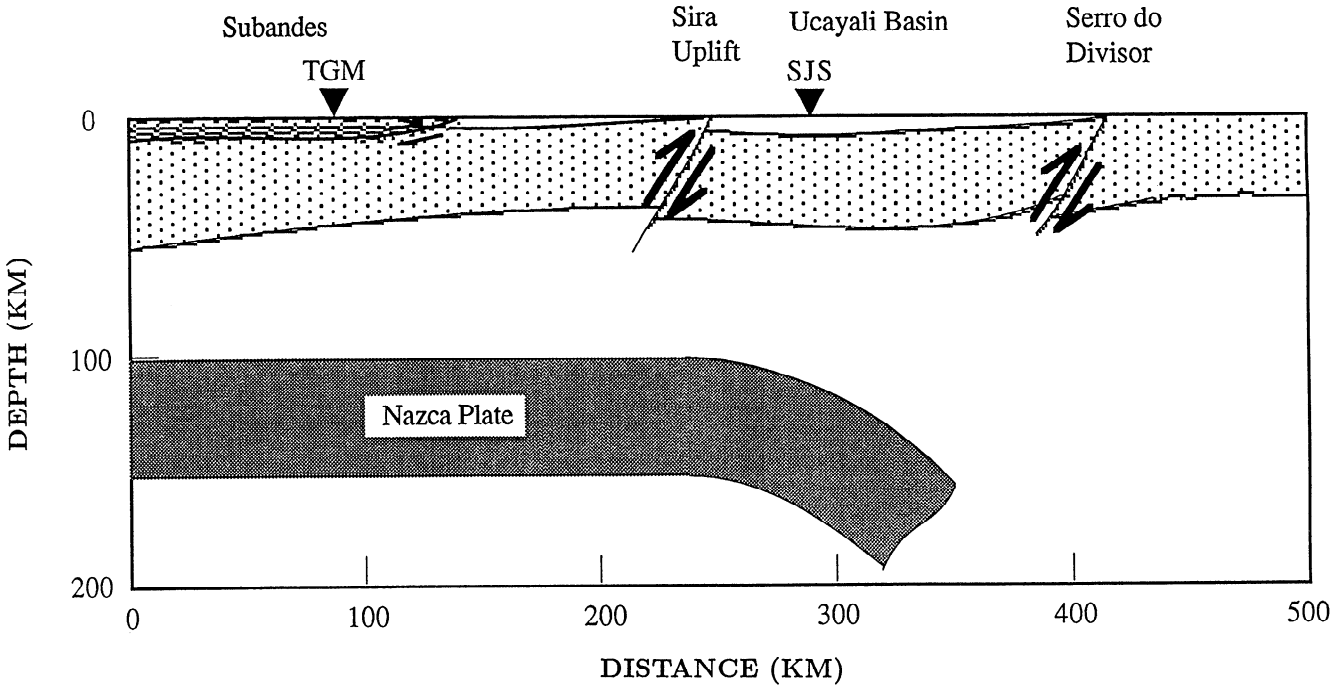


**Figure 13.** Speculative cross-section of Subandean zone and Ucayali basin along line B–B′ shown in preceding figures. The cross section is consistent with computed crustal structure as shown in Figures 11 and 12, but structures are interpolated through areas for which no seismic data are available. See text for further discussion.

sidence of the basin, or reverse fault uplift of crystalline basement. The seismic evidence [*Assumpção*, 1992] for reverse faulting at mantle depths in the Serra do Divisor indicates that faulting may be the more important process, although subsidence is probably also involved. (3) The crust appears to thin on the western edge of the Ucayali basin, suggesting that more than simple lithospheric flexure is involved in the tectonics of the advancing orogenic belt. It may be that mantle-penetrating faults of the thick-skin variety found for the Serro do Divisor also characterize at least parts of the western boundary of the Ucayali basin, notably in the regions of the Sira and Contamina uplifts.

**Acknowledgments.** This study was supported by NSF grants EAR-8720842, EAR-8720843, EAR-9018848 and EAR-901985. Map plots were done using GMT [*Wessel and Smith*, 1991].

## References

Allmendinger, R., D. Figueroa, E. Snyder, J. Beer, C. Mpodozis, and B. L. Isacks, Foreland shortening and crustal balancing in the Andes at 30° latitude, *Tectonics, 9*, 789-809, 1990.

Assumpção, M., The regional intraplate stress field in South America, *J. Geophys. Res., 97*, 11,889-11,903, 1992.

Beaumont, C., Foreland basins, *Geophys. J. R. Astron. Soc., 65*, 291-329, 1981.

Chapman, C.H., A first-motion alternative to geometrical ray theory, *Geophys. Res. Lett., 3*, 153-156, 1976.

Christensen, N.I., Seismic velocities, in *CRC Handbook of Physical Properties of Rocks*, edited by R.S. Carmichael, pp. 1-228, CRC Press, Boca Raton, Fla., 1982.

Clarke, T. J., and P. G. Silver, A procedure for the systematic interpretation of body wave seismograms, I., Application to Moho depth and crustal properties, *Geophys. J. Int., 104*, 41-72, 1991.

Clarke, T. J., and P. G. Silver, Estimation of crustal Poisson's ratio from broad band teleseismic data, *Geophys. Res. Lett., 20*, 241-244 1993.

Fielding, E., and T. Jordan, Active deformation at the boundary between the Precordillera and Sierras Pampeanas Argentina, and comparison with ancient Rocky Mountain deformation, *Mem. Geol. Soc. Am,. 171*, 143-163, 1988.

Ham, C. K., and L. J. Herrera, Jr., Role of Subandean fault system in tectonics of eastern Peru and Ecuador, in Backbone of the Americas, edited by O. E. Childs and B. W. Beebe, *AAPG Mem., 2*, 47-61, 1963.

James, D. E., Andean crustal and upper mantle structure, *J. Geophys. Res., 76*, 3246-3271, 1971.

Jordan, T. E., B. L. Isacks, R. W. Allmendinger, J. A. Brewer, V. A. Ramos, and C. L. Ando, Andean tectonics related to geometry of subducted Nazca plate, *Geol. Soc. Am. Bull., 94*, 341-361, 1983.

Lahr, J. C., HYPOELLIPSE/Version 2.0: A computer program for determining local earthquake hypocentral parameters, magnitude, and first motion pattern, *U.S. Geol. Surv. Open File Rep., 89-116*, 1992.

Lyon-Caen, H., P. Molnar, and G. Suárez, Gravity anomalies and flexure of the Brazilian shield beneath the Bolivian Andes, *Earth Planet. Sci. Lett., 75*, 81-92, 1985.

Mégard, F., Cordilleran Andes and marginal Andes: A review of Andean geology north of the Arica elbow, in *Circum-Pacific Orogenic Belts and Evolution of the Pacific Ocean Basin, Geophys. Monogr. Ser.*, vol 18, edited by J.W.H. Monger and J. Grancheteau, pp. 71-95, AGU, Washington, D.C., 1987.

Mingramm, A., A. Russo, A. Pozzo, and L. Cazau, Sierras Subandinas, in *Segundo Simposio de Geologia Regional*

*Argentina,* vol. 1, pp. 95-138, Academia Nacional de Ciencias, Cordoba, 1979.

Mooney, W. D., and L. W. Braile, The seismic structure of the continental crust and upper mantle of North America, in *The Geology of North America*, vol. A, *An Overview*, edited by A.W. Bally and A.R. Palmer, pp. 39-52, Geological Society of America, Boulder, Col., 1989.

Norabuena, E. O., J. A. Snoke, and D. E. James, Structure of the subducting Nazca plate beneath Peru, *J. Geophys. Res.*, in press, 1994.

Räsänen, M. E., J. S. Salo, and R. J. Kalliola, Fluvial perturbance in the western Amazon Basin: Regulation by long-term sub-andean tectonics, *Science, 238*, 1398-1401, 1987.

Smalley, R., Jr., J. Pujol, M. Regnier, J.-M. Chiu, J.-L. Chatelain, B. L. Isacks, M. Araujo, and N. Puebla, Basement seismicity beneath the Andean Precordillera thin-skinned thrust belt and its implications for crustal and lithosphere behavior, *Tectonics, 12*, 63-76, 1993.

Suárez, G. P., P. Molnar, and B. C. Burchfiel, Seismicity, fault plane solutions, depth of faulting, and active tectonics of the Andes of Peru, Ecuador, and southern Colombia, *J. Geophys. Res., 88*, 10,403-10,428, 1983.

Waters, K.H., *Reflection Seismology*, 538 pp., John Wiley, New York, 1987.

Wessel, P. and W. H. F. Smith, Free software helps map and display data, *Eos Trans. AGU, 72*, 441, 445-446, 1991.

---

D. E. James, Carnegie Institution of Washington, DTM, 5241 Broad Branch Rd., N.W., Washington, DC 20015.

J. A. Snoke, Department of Geological Sciences, Virginia Tech, Blacksburg, VA 24061-0420.

(Received November 5, 1992; revised August 12, 1993; accepted October 29, 1993.)